

Cite this: DOI: 10.1039/xxxxxxxxxx

# Towards a Spectroscopic Protocol for Unambiguous Detection of Quantum Coherence in Excitonic Energy Transport

Max Marcus,<sup>a‡</sup> George C. Knee,<sup>a</sup> and Animesh Datta<sup>a†</sup>

Received Date

Accepted Date

DOI: 10.1039/xxxxxxxxxx

www.rsc.org/journalname

The role of quantum effects in excitonic energy transport (EET) has been scrutinised intensely and with increasingly sophisticated experimental techniques. This increased complexity requires invoking correspondingly elaborate models to fit spectroscopic data before molecular parameters can be extracted. Possible quantum effects in EET can then be studied, but the conclusions are strongly contingent on the efficacy of the fitting and the accuracy of the model. To circumvent this challenge, we propose a witness for quantum coherence in EET that can be extracted directly from spectroscopic experimental data. We simulate a conceptually simple spectroscopic protocol capable of providing the necessary information to judge the feasibility of such an approach.

## 1 Introduction

The nature of energy transport in light-harvesting complexes, especially the role of quantum effects, is a topic of intense debate<sup>1–6</sup>. Central to this is the excited state dynamics of multichromophoric systems. These kinetics are usually studied with non-linear ultrafast optical spectroscopy, allowing for the investigation of the underlying processes in exciton energy transport (EET)<sup>7</sup>. Two-dimensional electronic spectroscopy (2DES) is sufficient to perform full tomography of the quantum process of excitonic dynamics within the singly-excited manifold of light-harvesting complexes and determine the precise values of the populations - as well as any quantum coherences between - energetic eigenstates<sup>8,9</sup> at the end of a dynamical process transforming any initial excited state. The question of the mere existence of quantum coherences, generated by a process acting on a particular input state is simpler and therefore potentially easier to answer. Our objective is to explore the possibility of a simpler spectroscopic scheme that is strictly easier than full process tomography and can still provide unambiguous evidence of quantum coherence. This work thus represents a step into an area of identifying quantum coherences in light-harvesting complexes, which is of fundamental interest but fraught with great difficulties both conceptual and practical. We hope to clarify some of these here.

While non-linear ultrafast spectroscopy experiments routinely

give qualitative insights into the complicated nature of the relevant processes, quantitative results are more difficult to obtain\*. In fact, the latter typically require theoretical modelling of the underlying physics and fitting such simulations to experiment then allows for the estimation of molecular parameters. While being a workable approach, the complicated nature of ultrafast spectroscopic experiments and the multitude of model parameters may allow for several possible interpretations. In general, this problem becomes severe as the experimental set-up of the spectroscopic experiment becomes more complicated.

Identifying quantum coherences in EET is difficult because of the major challenge of constructing tractable theoretical models for complex systems of chromophores interacting with various other degrees of freedom: while the chromophores interact with each other, so do the vibrational degrees of freedom of the protein scaffolding and the chromophores. This leads to a breakdown of common approximations (Born-Oppenheimer, Condon, etc.) making simulations expensive. Spectral congestion also hinders theoretical simulations and frustrates experiments. To overcome these difficulties experimental techniques have become ever more sophisticated by utilising multiple pulses, time delays, polarisations, and other properties of the incident light.

Any worthwhile discussion on the quantum effects in EET must begin with an unambiguous quantifier of quantum coherence† that is accessible experimentally. The size of the chromophores

<sup>a</sup> Department of Physics, University of Warwick, Gibbet Hill Road, Coventry, United Kingdom.

<sup>‡</sup> Present Address: Department of Chemistry, Physical & Theoretical Chemistry Laboratory, University of Oxford, South Parks Road, Oxford, United Kingdom. E-mail: max.marcus@chem.ox.ac.uk

<sup>†</sup> E-mail: animesh.datta@warwick.ac.uk

\* Sometimes called 'blobology'<sup>10</sup>

† While it has been said that "...coherence is theoretically well defined and also accessible to experimental quantification...",<sup>11</sup> the notion is by no means unique. Experimental accessibility then depends on which of these notions of coherence we seek to measure.

(a few nm) forbids any spatial resolution using far-field optical methods where the wavelengths are hundreds of nm. Notions of spatial quantum correlations are therefore not extractable<sup>‡</sup>. Temporal quantum correlations are the alternative. One proposal suggested identifying the quantum behaviour of the vibrational motions that drive EET via phonon anti-bunching<sup>6</sup>. This however requires coherent ultrafast *phonon* spectroscopy which remains challenging<sup>13</sup>. We therefore focus on a quantifier of quantum coherence that is experimentally accessible via non-linear ultrafast optical spectroscopy.

The notion of uniquely quantum correlations in time dates back to the work of Leggett and Garg, and their proposal for testing macroscopic realism (a certain classical limit of quantum mechanics) using inequality conditions<sup>14,15</sup>. Recent work has sharpened this notion and simplified this notion, culminating in the so-called No-Signalling-In-Time (NSIT) witness and its application in well-isolated engineered condensed matter quantum systems<sup>16–19</sup>. Intuitively, if a system undergoes a classical (possibly correlated) dynamical process, then interrupting with a non-invasive measurement and restarting it in the measured state would result in the same final state as if it had not been interrupted at all. On the contrary, interrupting the system undergoing a quantum dynamical process to measure and restart may result in a different final state. It is this difference between quantum and classical states that quantum coherence measures endeavour to capture<sup>20,21</sup>. Mathematically, they capture the off-diagonal elements in the density matrix as expressed in a preferred basis: in the context of NSIT, this basis is determined by the interrupting operation.. For a density matrix  $\rho$ , one such measure is given as,

$$R(\rho) = \frac{1}{2} \|\rho - \Gamma(\rho)\|_{\text{tr}}, \quad (1)$$

where  $\Gamma$  is the ‘non-invasive measurement’ interruption that excises all off-diagonal elements in  $\rho$  and  $\|X\|_{\text{tr}}$  is the trace norm defined as the sum of the singular values of  $X$ .

In this work we seek to probe  $R(\rho)$  spectroscopically, the basis is set by light pulses that create and probe excited states. In particular, non-zero off-diagonal elements in this basis are evidence against a Förster-type hopping in the exciton basis<sup>22</sup>. In principle therefore, a non-zero  $R(\rho)$  is evidence against models of EET mediated solely by the hopping of excitons, and in favour of quantum coherence playing a role. The same is true when the system under consideration is not isolated from its environment - as is the case for electronic excitations of chromophores in EET in relation to its vibrational modes, provided the Born approximation is satisfied at the time of this interruption. If not, as is likely in practice, subtleties arise<sup>23</sup>.

The paper is organised as follows. In Sec. 2, we begin by adapting our previous theoretical work on a general system coupled to a bath to suit the discussion of EET. By deriving an expression for the No-Signalling-In-Time (NSIT) witness we will show that all quantities needed for its evaluation are readily available from

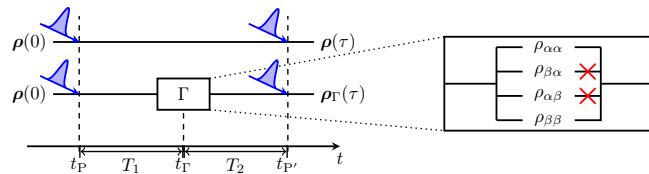


**Fig. 1** Schematic depicting the proposed spectroscopic protocol. Two identical samples in identical states are exposed to the same pulses at the same time, with one being interrupted by the operation  $\Gamma$ . This operation is instantaneous and amounts to quantum population tomography and re-preparation without the off-diagonal elements (quantum coherence elements). The states are compared at the end.

spectroscopic techniques. Moreover, we will introduce a protocol that is - in principle - able to provide a numerical value for the NSIT witness via experiment. We will then introduce a dimer model in Sec. 3 to simulate the required protocol and use it in numerical studies on allophycocyanin, a molecular system commonly used as a model substance for EET. The discussion of the numerical results and the comparison with theoretical expectations will show a discrepancy which is then subsequently discussed in light of the validity of the spectroscopic approach. We will finish the paper with a summary and an outlook on possible future avenues to experimentally measure the NSIT witness while minimising the experimental effort.

## 2 The No-Signalling-In-Time Witness

Previous work has considered the concept of quantum witnesses in systems coupled to baths<sup>23,24</sup>. We derived three distinct witnesses of quantum coherence containing information about the presence of coherences between or within the system and bath. In this paper we will focus on the second of these witnesses, labelled  $W^b$ , which provides information about the presence of coherences in time between system states. Mathematically,

$$R(\rho(t)) \geq 2W^b(t; T), \quad (2)$$

where  $T$  is the total time of the experiment. positive value of  $W^b(t; T)$  is thus an unambiguous witness of quantum coherence in EET. We will present an experimental scheme for obtaining  $W^b(t; T)$ . We will briefly revisit the idea behind this witness; for a more detailed discussion we refer to our previous work<sup>23</sup>.

Consider a system coupled to a bath. We can partition the overall state at any time,  $t$ , as,

$$\rho_{\text{SB}}(t) = \rho_{\text{S}}(t) \otimes \rho_{\text{B}}(t) + \gamma_{\text{SB}}(t), \quad (3)$$

where  $\gamma_{\text{SB}}(t)$  is the correlation between the system and the bath. A general state subject to unitary evolution will then propagate between two times,  $t_P$  and  $t_{P'}$  as (see Fig. 1),

$$\rho_{\text{SB}}(t_{P'}) = U(t_{P'}, t_P) \rho_{\text{SB}}(t_P) U^\dagger(t_{P'}, t_P) = \mathcal{U}_{t_{P'}, t_P}[\rho_{\text{SB}}(t_P)]. \quad (4)$$

In this work we will adopt the Born approximation. This assumption is sufficient to allow the evolution to be partitioned at time  $t_\Gamma$  and we may write,

$$\rho_{\text{SB}}(t_{P'}) = \mathcal{U}_{t_{P'}, t_\Gamma} \circ \mathcal{U}_{t_\Gamma, t_P}[\rho_{\text{SB}}(t_P)] \quad (5)$$

<sup>‡</sup> Except perhaps with coherent 2D photoemission electron microscopy (PEEM) which provides 50-nm spatial resolution<sup>12</sup>.

If the state at  $t_\Gamma$  is not changed by some intervention then Eqs. (3) and (4) will be the same. If, however, some operation  $\Gamma$  is performed at time  $t_\Gamma$  then the state,

$$\rho_{\text{SB}}^\Gamma(t_{\text{P}}) = \mathcal{U}_{t_{\text{P}}, t_\Gamma} \circ \Gamma \circ \mathcal{U}_{t_\Gamma, t_{\text{P}}} [\rho_{\text{SB}}(t_{\text{P}})], \quad (6)$$

may differ from the state in Eq. (4) and detecting that difference may serve as a witness to the quantum coherence of the state at time  $t_\Gamma$ . This assumes that  $\Gamma$  is *non-invasive* in that it excises the off-diagonal elements in  $\rho_{\text{SB}}(t_\Gamma)$  instantaneously without affecting the subsequent dynamics in any way<sup>14,23</sup>. If at time  $t_{\text{P}}$  we measure the system then we can find an observable as,

$$\mathcal{O}(t_{\text{P}}) = \text{tr} \{ (M \otimes \mathbf{I}_{\text{B}}) \rho_{\text{SB}}(t_{\text{P}}) \} = \text{tr}_{\text{S}} [M \rho_{\text{S}}(t_{\text{P}})], \quad (7)$$

where the bath was traced out. Comparing the two observables with and without the operation  $\Gamma$  then gives us a measure for the effect of  $\Gamma$  and we find,

$$W^b(t_\Gamma; \tau = t_{\text{P}} - t_{\text{P}}) = \left| \text{tr}_{\text{S}} \{ M \text{tr}_{\text{B}} [\mathcal{U}_{t_{\text{P}}, t_\Gamma} \gamma_{\text{SB}}(t_\Gamma)] \} + \text{tr}_{\text{S}} \{ \mathcal{E}(M) \rho_{\text{S}}(t_\Gamma) \} - \text{tr}_{\text{S}} \{ \mathcal{E}^\Gamma(M) \rho_{\text{S}}(t_\Gamma) \} \right|, \quad (8)$$

where  $\mathcal{E}$  is a mapping containing the evolution of the coupled system-bath and the measurement performed on the system.  $\mathcal{E}^\Gamma$  is defined in the same manner, with the operation  $\Gamma$  preceding the natural evolution. We refer the reader to previous work for an in-depth discussion and more rigorous derivation of Eq. (7). The Born approximation has two effects on our witness: firstly, it forces  $\gamma_{\text{SB}}(t) = 0 \forall t$  causing the first term to vanish, and secondly the underlying evolution and measurement mappings,  $\mathcal{E}(M)$  and  $\mathcal{E}^\Gamma(M)$  will be identical with the exception of the operation  $\Gamma$  at  $t_\Gamma$  for the second case. As a result,  $W^b$  reports exclusively on coherences between system eigenstates in the basis determined by  $\Gamma$ . For brevity, we will suppress the time arguments on  $W^b$  in the following.

The excited states which are preparable and measurable in spectroscopy are determined by the relationship of the light pulses with the matter. In order to implement  $\Gamma$ , we may choose to measure and (re)prepare in an orthogonal basis of excited states: here will focus on the energy eigenbasis of the system (i.e. the exciton basis), and will look to achieve this by tuning light pulses to exclusively target one transition or the other.

As such,  $W^b$  gives the difference in the populations of one eigenstate of the system when interrupted at time  $t_\Gamma$ . A quantum process formalism is particularly useful here as it allows us to relate any reduced density matrix of the system at time  $t_{\text{P}}$  to its state at time  $t_{\text{P}}$  as,

$$\rho_{\text{S}}(t_{\text{P}}) = \chi(t_{\text{P}} - t_{\text{P}}) \rho_{\text{S}}(t_{\text{P}}). \quad (9)$$

$\chi(t)$  is a degree-4 tensor called the process tensor<sup>7</sup>. This allows us to express any element of the density matrix of the state at any time  $t > t_{\text{P}}$  as,

$$\rho_{ij}(t) = \sum_{pq} \chi_{ijpq}(t - t_{\text{P}}) \rho_{pq}(t_{\text{P}}). \quad (10)$$

This allows us to express the unitary evolution in terms of the

process tensor and we can write,

$$\text{tr}_{\text{S}} \{ \mathcal{E}(M) \rho_{\text{S}}(t_\Gamma) \} = \sum_{pq} \chi_{iipq}(t_{\text{P}} - t_\Gamma) \rho_{pq}(t_\Gamma), \quad (11)$$

$$\text{tr}_{\text{S}} \{ \mathcal{E}^\Gamma(M) \rho_{\text{S}}(t_\Gamma) \} = \sum_{pq} \chi_{iipq}(t_{\text{P}} - t_\Gamma) \Gamma [\rho_{pq}(t_\Gamma)], \quad (12)$$

where  $M = |i\rangle \langle i|$  measures the population in the eigenstate  $|i\rangle$ . Since the state is initially prepared at time  $t_{\text{P}}$  then we can further expand,

$$\text{tr}_{\text{S}} \{ \mathcal{E}(M) \rho_{\text{S}}(t_\Gamma) \} = \sum_{pqrs} \chi_{iipq}(t_{\text{P}} - t_\Gamma) \chi_{pqrs}(t_\Gamma - t_{\text{P}}) \rho_{rs}(t_{\text{P}}), \quad (13)$$

$$\text{tr}_{\text{S}} \{ \mathcal{E}^\Gamma(M) \rho_{\text{S}}(t_\Gamma) \} = \sum_{pqrs} \chi_{iipq}(t_{\text{P}} - t_\Gamma) \Gamma [\chi_{pqrs}(t_\Gamma - t_{\text{P}}) \rho_{rs}(t_{\text{P}})]. \quad (14)$$

Choosing the operation  $\Gamma$  such that it eliminates all coherences in the system at time  $t_\Gamma$  then alters Eq. (13) to give,

$$\text{tr}_{\text{S}} \{ \mathcal{E}^\Gamma(M) \rho_{\text{S}}(t_\Gamma) \} = \sum_{prs} \chi_{iipr}(t_{\text{P}} - t_\Gamma) \chi_{pprs}(t_\Gamma - t_{\text{P}}) \rho_{rs}(t_{\text{P}}). \quad (15)$$

In Eq. (12) we can contract the two process tensors into one for the entire time. Note that we cannot do that in Eq. (14) as the summation is incomplete. We can then combine Eqs. (12) and 14) to express our witness as,

$$W^b = \left| \sum_{rs} \left\{ \chi_{iirs}(t_{\text{P}} - t_{\text{P}}) - \sum_p \chi_{iipr}(t_{\text{P}} - t_\Gamma) \chi_{pprs}(t_\Gamma - t_{\text{P}}) \right\} \rho_{rs}(t_{\text{P}}) \right|. \quad (16)$$

Note that this quantity depends on the state  $|i\rangle$ , the projection onto which we chose to be our final measurement. Intuitively, this definition captures the following: the first term within the summation captures all dynamics from  $|r\rangle \langle s|$  at  $t_{\text{P}}$  to  $|i\rangle \langle i|$  at  $t_{\text{P}}$  via all possible routes, while the second term excludes any dynamics between these arising from coherences in the energy basis at some arbitrarily chosen intermediate time  $t_\Gamma$ . If those two terms cancel out, then there is no dynamics via states involving coherence in the energy basis at  $t_\Gamma$  indicating that the dynamics is, indeed, incoherent. Any non-zero value for  $W^b$  then indicates that coherences are indeed present at time  $t_\Gamma$ . We can simplify the witness further by starting, for instance, with  $\rho(t_{\text{P}}) = |\alpha\rangle \langle \alpha|$ . This will become useful below when we adapt the witness to suit a pump-probe experiment for a dimer system.

We will now proceed to obtain an explicit expression for  $W^b$  for a dimer model system and derive a spectroscopic protocol which is, in principle, capable providing the necessary elements of the process tensor without the need of full quantum process tomography (QPT) thereby reducing the experimental (and computational) cost significantly.

## 3 Dimer Model System

### 3.1 System-Bath Hamiltonian

We model the excited state dynamics of a dimer coupled to a bath of harmonic oscillators, one per site. The corresponding Hamilto-

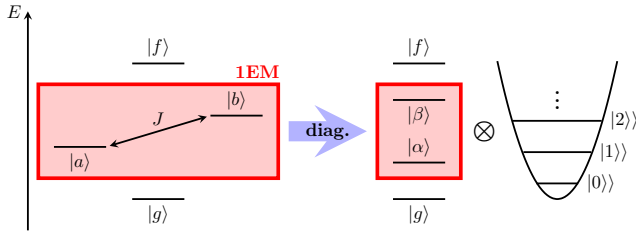


**Fig. 2** Schematic depiction of the basis set used. The site basis (left) is diagonalised and expanded by local harmonic oscillators. The excitonic and phononic degrees of freedom are then coupled via  $\hat{H}_{\text{SB}}$ . The EET dynamics occur in the singly excited manifold (1EM).

nian takes the form of a Frenkel-Holstein Hamiltonian,

$$\hat{H}_S = \sum_{i=\{a,b\}} \varepsilon_i \hat{a}_i^\dagger \hat{a}_i + J \left( \hat{a}_a^\dagger \hat{a}_b + \hat{a}_b^\dagger \hat{a}_a \right) \quad (17)$$

$$\hat{H}_B = \hbar \sum_{i=\{a,b\}} \omega_i \left( \hat{b}_i^\dagger \hat{b}_i + \frac{1}{2} \right) \quad (18)$$

$$\hat{H}_{\text{SB}} = -\hbar \sum_{i=\{a,b\}} \omega_i g_i \hat{a}_i^\dagger \hat{a}_i \left( \hat{b}_i^\dagger + \hat{b}_i \right), \quad (19)$$

where  $a$  and  $b$  are the site indices and  $\hat{a}_i^\dagger/\hat{a}_i$  and  $\hat{b}_i^\dagger/\hat{b}_i$  are exciton and phonon creation/annihilation operators, respectively. The dimensionless exciton-phonon coupling parameter,  $g_i$ , is related to the Huang-Rhys parameter,  $S_i$ , as  $S_i = g_i^2/2$ . For a more detailed discussion of the Frenkel-Holstein model see the work by Barford et al.<sup>25–27</sup>

The basis states of the uncoupled Hamiltonian, as shown in Fig. 2 (left), are the electronic states,  $\{|g\rangle, |a\rangle, |b\rangle, |f\rangle\}$  and the ladder of localised phonon states of the harmonic oscillator,  $\{|n\rangle_m\}$  of  $n$  phonons on site  $m$ . We construct a basis by diagonalizing the uncoupled Hamiltonian, resulting in product states linking one electronic eigenstate to a ladder of delocalised phonons. The electronic eigenstates are the electronic ground state,  $|g\rangle$ , the two states forming the singly excited state manifold (1EM),  $|\alpha\rangle$  and  $|\beta\rangle$ , and the state forming the doubly excited state manifold (2EM),  $|f\rangle$ .  $|\alpha\rangle$  and  $|\beta\rangle$  correspond to the bonding and antibonding orbitals of a dimer system if  $J < 0$ .

We are interested in the excited state dynamics occurring in the singly-excited manifold (1EM) of the system under consideration. Experimentally, non-linear spectroscopic techniques are commonly used to elucidate these dynamics and to determine the existence of quantum coherences between states. Most prominently, two-dimensional electronic spectroscopy (2DES) is used to detect off-diagonal peaks in the spectra, oscillations of which are commonly interpreted as signatures for quantum coherences<sup>1</sup>. Note that, while such oscillations are consistent with a quantum coherent model, they could also be consistent with certain classical models. Experimentally simpler is pump-probe spectroscopy in which the sample is exposed to two short pulses of light with a time delay,  $\tau$ , where the first pulse (pump) generates an excited state in the sample which is then measured by the second pulse (probe). We will use this spectroscopic set-up to develop a protocol making our previous theoretical findings experimentally accessible. Somewhat counterintuitively, our protocol allows

quantum coherence to be revealed (if it exists) without the need for more complicated types of spectroscopy, such as 2DES. This is because quantum coherence is not probed directly, but only indirectly through its implicit deletion under the  $\Gamma$  operation, which we aim to achieve using only two-pulse pump-probe experiments. Moreover, our protocol allows for classical models (that have zero quantum coherence) to be decisively ruled out.

### 3.2 Quantum Coherence Witness

Full quantum process tomography (QPT) is, while in principle possible, very expensive as the number of unknowns scales as  $d^4 - d^2$ , where  $d$  is the dimensionality of the Hilbert space of the system. In its current form, our witness (Eq. (15)) requires far less than full knowledge of the process tensor, albeit for two distinct evolution periods. However, some additional assumptions can further reduce the workload significantly: (i) the most drastic assumption (and most difficult one to realise in experiment) is that at  $t_p$  the system is in the state  $|\alpha\rangle$ . Then Eq. (15) reduces to,

$$W^b = \left| \chi_{iia\alpha}(t_{p'} - t_p) - \sum_p \chi_{iipp}(t_{p'} - t_\Gamma) \chi_{pp\alpha\alpha}(t_\Gamma - t_p) \right|, \quad (20)$$

as  $\rho_{\alpha\alpha}(t_p) = 1$ . A similar assumption is required to enable us to achieve  $\Gamma$ : namely, the ability to selectively prepare and measure  $|\alpha\rangle$  and  $|\beta\rangle$ . (ii) if we further assume trace preservation (no excitonic dissipation) then preparing an eigenstate initially imposes a normalisation constraint on certain elements of the process tensor, namely,

$$\sum_i \chi_{iipq}(t' - t) = 1 : \quad \forall p, q, \quad (21)$$

which allows us to write our witness for a dimer system with eigenstates  $|\alpha\rangle\langle\alpha|$  and  $|\beta\rangle\langle\beta|$  for example as,

$$W^b = |\chi_{\alpha\alpha\alpha\alpha}(\tau) + \chi_{\alpha\alpha\alpha\alpha}(T_1)(1 - \chi_{\alpha\alpha\alpha\alpha}(T_2)) + \chi_{\beta\beta\beta\beta}(T_2)(1 - \chi_{\alpha\alpha\alpha\alpha}(T_1)) - 1|, \quad (22)$$

where  $T_1 = t_\Gamma - t_p$ ,  $T_2 = t_{p'} - t_\Gamma$ , and  $\tau = T_1 + T_2$ . The significance of Eq. (21) is that it allows us to judge the existence of coherence within the system by merely determining two elements of the process tensor at three distinct times. This is a significant reduction of the workload compared to full quantum process tomography.

As the excited state dynamics is governed by the full Hamiltonian in Eqs. (16) - (18) it is possible to calculate an idealised, theoretical process tensor directly from the resulting reduced evolution. We will outline this below. Since extracting quantum coherences experimentally is our eventual endeavour, we will continue in Sec. 3.4 to derive a spectroscopic protocol which is, in principle, capable of providing the required information. We will then numerically simulate these experiments in Sec. 4 (using a realistic model of light-matter interactions) and present the results. The idealised calculations introduced next will serve as a benchmark for those simulations.

### 3.3 Idealised Theoretical Process Tensor

Simulating the required spectroscopic experiments is computationally expensive for several reasons.

Firstly, there are the exponential memory requirements needed to represent systems with more structure. Even a small increase in the energy cutoff for each harmonic oscillator of the environment, or in the number of chromophores in the system itself that we model, can result in the simulations being dramatically more costly. In fact, the size of the Hilbert space scales exponentially with the number of chromophores and phonons considered. For a system of  $N_{\text{sites}}$  sites with localised harmonic oscillators with  $N_{\text{phon}}$  vibrationally excited states the Hilbert space of all excitations has the dimensionality

$$d = N_{\text{sites}}^2 (N_{\text{phon}} + 1)^{N_{\text{sites}}}. \quad (23)$$

For instance, for a Fenna-Matthews-Olsen complex with 7 sites and 9 phonons on each site (10 vibrational levels for a single harmonic oscillator),  $d = 4.9 \times 10^8$ , which would require on the order of  $10^{34}$  experiments for full quantum state tomography. For our proof-of-concept simulations we have therefore chosen a rudimentary model of a light harvesting complex: far more sophisticated approaches are possible by judicious choices of approximations and/or approximate solvers.

Secondly, the need for isotropic averaging to simulate realistic samples exacerbates the situation, since a direct simulation of different orientations implies an overhead multiplier of the number of samples needed. We estimate this number to be in the 1000s. The independence of the different orientations, however, make the simulation highly parallelizable.

Thirdly, the time-dependent nature of the problem and the different time-scales involved makes integrating the dynamics much more difficult. However, to benchmark our calculations and judge the quality of the simulations and approximations made we can calculate the process tensor directly for the model Hamiltonian used - essentially by replacing the semi-classical light-matter interaction with perfect preparation and measurement of the two excited states that we wish to target.

We will now continue by laying out how to simulate spectroscopic experiments and how these can be used to determine the process tensor of excited state dynamics to inform us about a feasible spectroscopic protocol capable of extracting  $W^b$  from experimental data.

### 3.4 Excited State Dynamics

The dimer model introduced in Sec. 3.1 is subjected to a (time-dependent) classical field given by,

$$\begin{aligned} \hat{V}(t) &= - \sum_n \sum_i \hat{\mu}_i \cdot \mathbf{E}_n(t) \\ &= - \sum_{ni} \hat{\mu}_i \cdot \mathbf{e}_n \left( \hat{a}_i^\dagger + \hat{a}_i \right) \exp \left( - \frac{(t - t_n)^2}{2\sigma_n^2} \right) \left[ e^{-i\omega_n t} + e^{i\omega_n t} \right], \end{aligned} \quad (24)$$

where a Gaussian envelop with central pulse time  $t_n$  and width  $\sigma_n$  is convoluted with an oscillating electric field.  $n$  runs over

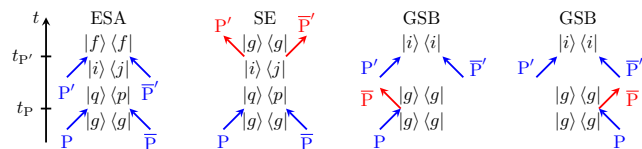


**Fig. 3** First-order non-linear optoelectronic processes in a general system when interacting with two pulses (P and P') at two distinct times shown as double-sided Feynman Diagrams (DSFDs). ESA: Excited State Absorption; SE: Stimulated Emission; GSB: Ground-State Bleach. Each process involves the 1EM.

the pulses, while  $i$  labels the states.  $\mathbf{e}_n$  is the polarisation of the pulse with a magnitude of  $|\mathbf{e}_n| = \eta_n$  being the intensity. When interacting with the system the oscillating field will have one term significantly closer to resonance than the other. While computationally not less expensive, making the Rotating Wave Approximation (RWA), which neglects the off-resonant oscillation, makes the theoretical calculation of transition probability amplitudes easier and we will use the RWA throughout this work.

To simulate spectroscopic experiments we need to initialise the system and environment before any interaction with the pulses. While straightforward to incorporate thermalized state at finite temperatures, we have chosen to initialise the system and environment in their respective groundstate, in effect leading to simulations of experiments at 0 K. The interaction of two subsequent pulses with a sample initialised in this way will give rise to a multitude of processes between the ground and excited states. To first-order these are either of Excited State Absorption (ESA), Stimulated Emission (SE), or Ground-State Bleach (GSB), see Fig. 3. Each of these processes will contribute to the overall signal observed in a pump-probe experiment. Following Yuen-Zhou et al.<sup>28</sup>, we can calculate these contributions by considering the transition probability amplitudes,

$$\Omega_{ij}^p = \tilde{E}_p(\omega_{ij}) \mu_{ij} \cdot \mathbf{e}_p, \quad (25)$$

where  $\tilde{E}_p(\omega_{ij})$  is the Fourier-transform of the Gaussian pulse (Eq. 23),  $\mu_{ij}$  is the transition dipole moment between states  $|j\rangle$  to  $|i\rangle$  and  $\mathbf{e}_p$  is the polarization of the pulse. The dynamics occurring within the system between the two pulses are quantified by the process tensor describing the natural evolution. Each contribution (ESA/SE/GSB) can then be expressed as the product of three different factors summed over each possible combination of states: 1. a factor for exciting the true ground state with a given pulse (P) into a given excited 'state'; 2. a factor representing transition from that 'state' into another 'state' within the 1EM under natural evolution; and 3. a factor of reaching a given target 'state' under interaction with the second pulse (P'). For instance, for the ESA these contributions are given as,

$$S_{\text{ESA}}(\tau) = \sum_{pqij} \left[ \Omega_{qs}^p \Omega_{gp}^p \times \chi_{ijqp}(\tau) \times \Omega_{fi}^{p'} \Omega_{jf}^{p'} \right], \quad (26)$$

where the factors have been expressed using the transition probability amplitudes. Note that the 'states' are sometimes non-Hermitian operators, and their appearance is an idiosyncrasy of perturbation theory.

Similar expressions can be formulated for the SE and GSB as,

$$S_{SE}(\tau) = - \sum_{ijpq} \Omega_{gi}^{P'} \Omega_{qg}^P \Omega_{gp}^{P'} \Omega_{jq}^P \chi_{ijqp}(\tau), \quad (27)$$

$$S_{GSB} = - \sum_{ip} \Omega_{ig}^{P'} \Omega_{gp}^P \Omega_{pg}^{P'} \Omega_{gi}^P, \quad (28)$$

where  $i, j, p, q$  label states within the 1EM. The total signal of a general pump-probe experiment is then given as the sum of these contributions and will, in general, be a function of all elements of the process tensor, 16 for a two-level 1EM. In order to be experimentally (and computationally) cheaper than QPT the number of these unknowns has to be reduced by making judicious choices of experimental parameters, which will directly inform the simulation of the resulting experiments. Furthermore, in order for our quantum witness  $W^b$  to inform on the presence of coherences within the natural evolution we have to explicitly exclude the possibilities of creating such coherences with the light pulses. This is because the witness only informs on the presence of any coherence, without regard as to where they have arisen from. We therefore require the initially prepared state to be an eigenstate, and  $p = q$  in the previous equations. This constraint eliminates eight elements in the process tensor. By tailoring the light field to only prepare and probe excitonic eigenstates we can eliminate a further four contributions, reducing the equations above to four unknown elements, namely the population-to-population elements,  $\chi_{iipp}$ . The equations then reduce to,

$$\mathcal{S}_{ESA}(\tau) = \sum_{pq} \Pi_{fq}^{P'} \Pi_{pg}^P \chi_{qqpp}(\tau), \quad (29)$$

$$\mathcal{S}_{SE}(\tau) = - \sum_{pq} \Pi_{gq}^{P'} \Pi_{pg}^P \chi_{qqpp}(\tau), \quad (30)$$

$$\mathcal{S}_{GSB}(\tau) = - \sum_{pq} \Pi_{gq}^{P'} \Pi_{pg}^P, \quad (31)$$

where for our dimer model  $p, q \in \{\alpha, \beta\}$ . To find the four elements of the process tensor we require four linearly-independent signals containing information about the excited state dynamics within our electronic dimer system. In fact, we can write,

$$\begin{aligned} \mathcal{S}(\tau) &= \mathcal{S}_{ESA}(\tau) + \mathcal{S}_{SE}(\tau) + \mathcal{S}_{GSB}(\tau) \\ &= \sum_{pq} \left[ \Pi_{fq}^{P'} \Pi_{pg}^P - \Pi_{gq}^{P'} \Pi_{pg}^P \right] \chi_{qqpp}(\tau) - \sum_{pq} \Pi_{gq}^{P'} \Pi_{pg}^P \\ &= \sum_{qp} M_{qp}(P', P) \chi_{qqpp}(\tau) - G(P', P). \end{aligned} \quad (32)$$

Selecting four different pulse sequences  $(P', P)$  with the same delay time then allows us to re-write Eq. (31) in vectorised form as,

$$\mathbf{S}(\tau) = \mathbf{M} \tilde{\chi}(\tau) - \mathbf{G}, \quad (33)$$

where  $\tilde{\chi}(\tau)$  is the vectorised reduced process tensor with the four entries mentioned above. In order to recover the process tensor elements from this equation we require the matrix  $\mathbf{M}$  to be non-singular and well-conditioned. As the elements of the matrix depend directly on the pulses used, their choice is crucial in order to recover an invertible matrix.

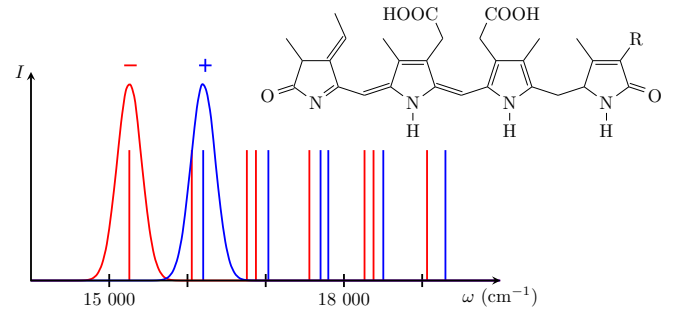


**Fig. 4** Theoretical absorption energies of a dimer not coupled to the environment ( $\hat{H}_{SB} = 0$ ) and structural formula of the chromophore phycoerythrobilin ( $R = C_2H_3$ ). The pulses targeting the vibrationless excited states are indicated, as well.

### 3.5 Choice of Pulse Sequences

Eq. (32) is derived on the assumption that we can create and measure an eigenstate of the system under investigation, i.e. pulses of light selectively interact with only one electronic transition. We therefore need to ensure that the pulses have large spectral overlap with one transition and vanishing overlap with all others. For a dimer with two electronic states and no environment the choice of pulses is straight-forward: by de-tuning the pulses in frequency from the two transitions in such a way that the energetic gap between the pulses is larger than between the transitions the cross-talk can be minimised. In such a way the transition probability amplitudes to coherent states vanish and the approximations made above become exact, allowing for an accurate and precise recovery of the process tensor elements. For a system coupled to a bath both transitions for a dimer acquire a vibronic tail, which can overlap. Fig. 4 shows the schematic absorption spectra of commonly encountered chemical species in the  $\hat{H}_{SB} = 0$  limit. The two vibrational manifolds of the two electronic transitions are shown in red and blue. Clearly visible is that even in the case of vanishing coupling the tails overlap significantly. We can therefore not target electronic transitions without exciting coherences while being broadband with respect to the vibrational degrees of freedom.

This directly impacts the assumption we made above: by not being able to exclude the possibility of creating coherences with the light-pulse the witness will report on coherences generated by the light as well as the system dynamics, without distinguishing between the two. This is the 'Fourier transform' of a problem commonly encountered in experimental spectroscopy: in order to exclude the possibility of higher-order processes the incident light pulse needs to be short such that excitations occur on a timescale much shorter than the natural evolution. It is within these constraint of the Fourier transform that the pulses need to be chosen: ideally they are delta pulses in both, frequency and time.

For the purpose of this work we have made the pulses resonant with the electronic transitions and labelled them '+' and '-' for the higher and lower energy transitions, respectively. With this toolbox of two pulses we can construct four distinct pump-probe experiments and we will now discuss how these can be used to measure the witness derived above.

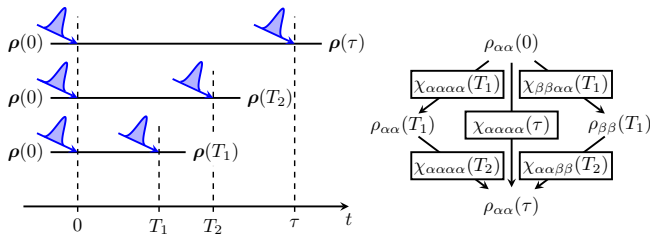


**Fig. 5** Schematic showing our proposed experimental implementation of the protocol. Three identical examples are pumped with the same pulse and probed at different times to extract population-to-population elements of the process tensor. Comparing the result from two distinct times,  $T_1$  and  $T_2$ , making up an overall time,  $\tau$ , allows a statement about the presence of quantum coherences at  $T_1$ .

### 3.6 Spectroscopic Protocol

As laid out in Sec. 3.2 we require the population-to-population elements of the process tensor for three distinct natural evolution times:  $T_1$ ,  $T_2$ , and  $\tau = T_1 + T_2$ . According to Sec. 3.4 we can measure these elements using pump-probe spectroscopy if we choose the pulses judiciously (see Sec. 3.5). For a two-level system with two targeted pulses we can construct four pump-probe experiments that in principle fulfil these requirements. The conceptual derivation of the witness in Sec. 2 required the deletion of all coherences within the systems at time  $t_1$  (see Fig. 1). While possible in principle, the design of such pulse(s) is outside of the scope of this work. See also the work of Moreira and Semião<sup>29</sup>, where a different mathematical operation is proposed in order to test a distinct but related witness, but is not translated into an ostensibly-feasible spectroscopic operation. Due to the discussion in Sec. 3.2,  $\Gamma$  can be replaced with partial quantum process tomography at three distinct delay times, as laid out above. The experimental set up therefore breaks down into three distinct experiments per pulse sequence (see Fig. 5): three identical samples are exposed to the same pump-pulse and probed with the same pulse at the three delay times mentioned above. The results of the four different pulse sequences allows for the recovery of the population-to-population elements at different delay times which allows for the calculation of the witness. Alternatively, these elements can be determined at different times and for each triple  $\tau = T_1 + T_2$  the witness can then be calculated.

## 4 Numerical Results

We now present numerical simulations of the spectroscopic protocol set out above on a model system often used to research EET, namely a dimer of phytoerythrobilin, a chromophore found in allophycocyanin. Details on the computational methodology can be found in App. A. We will use two different methods to achieve pulse selectivity: first by utilising the polarisation of pulses and the relative orientation of the transition dipole moments in a single dimer experiment, and secondly by averaging isotropically over an ensemble of dimers and using energetic targeting of the transitions. The values for the parameters in the Hamiltonians in Eqs. (16) - (18) are given in Tab. 1.

**Table 1** Parameters used to simulate a dimer of phytoerythrobilin molecules for the system, bath, and light pulses

Parameter (unit)	Value
$\epsilon_a$ (cm <sup>-1</sup> )	15 300
$\epsilon_b$ (cm <sup>-1</sup> )	16 200
$J$ (cm <sup>-1</sup> )	-162
$\omega_a$ (cm <sup>-1</sup> )	800
$\omega_b$ (cm <sup>-1</sup> )	1500
$g_a$	0.1
$g_b$	0.15
$\sigma_p$ (cm <sup>-1</sup> /fs)	322/103
$\eta_p$ (eV ps/D)	$5 \times 10^{-6}$

### 4.1 Single Dimer Spectroscopy

As shown in Fig. 4 the vibronic progressions for allophycocyanin overlap significantly, with the first vibrationally excited state of the  $\alpha$ -manifold almost degenerate with the vibrational ground state of the  $\beta$ -manifold. As such, pulse selectivity by tuning the frequency and width of the pulses is difficult to achieve: while possible in principle, the narrowness in frequency would lead (conventionally) to a very long pulse (on the order of several 100 fs) which would mix the natural evolution with processes induced by the continuous action of the pulse, rendering our analysis useless. However, for the single dimer we can choose the polarisation of the pulses to be aligned with one transition each, leading to the other transition being dark to that respective pulse (due to the mutual orthogonality of the two transitions). We can thus overcome the restriction imposed by the width of the pulse in frequency. This has a direct consequence on the expansion of the recorded signal. Starting from Eq. (31) we can simplify the expression by considering that the pump only excites into a given state, say  $|i\rangle$ , while the probe,  $P'$ , only excites into state  $|j\rangle$ . Then,

$$\mathcal{S}(\tau) = \Pi_{fj}^{P'} \Pi_{ig}^P \chi_{\bar{j}ji}(\tau) - \Pi_{gj}^{P'} \Pi_{ig}^P \chi_{jii}(\tau) - \Pi_{gj}^{P'} \Pi_{ig}^P, \quad (34)$$

where  $\bar{j}$  represents the state that would need to be excited to achieve the transition from  $|j\rangle$  to  $|f\rangle$ . For our dimer model we have  $i, j \in \{\alpha, \beta\}$  and we can write four equations which separate into two systems of two equations with two unknowns each. For  $j = i$  the pump and probe pulses are identical (P and P), whereas for  $j \neq i$  they are the opposites of each other (P and -P). We therefore find,

$$\mathcal{S}^{P,P}(\tau) = \Pi_{fj}^P \Pi_{ig}^P \chi_{jji}(\tau) - \Pi_{gi}^P \Pi_{ig}^P \chi_{iii}(\tau) - \Pi_{gi}^P \Pi_{ig}^P, \quad (35)$$

$$\mathcal{S}^{-P,P}(\tau) = \Pi_{fi}^P \Pi_{ig}^P \chi_{iii}(\tau) - \Pi_{gj}^P \Pi_{ig}^P \chi_{jjj}(\tau) - \Pi_{gj}^P \Pi_{ig}^P. \quad (36)$$

As is shown explicitly in App. A these two equations will be linearly dependent for perfectly polarisation selective pulses, meaning the inversion of  $\mathbf{M}$  fails. Indeed, numerical simulations lead to conditions numbers of order  $10^6$  and above (the equations are only nearly linearly dependent due to numerical inaccuracies). This linear dependence is due to the equivalence of the  $|g\rangle$  to  $|i\rangle$  and  $|j\rangle$  to  $|f\rangle$  transitions, as the transition probability for both transitions will be identical for a given pulse. One might imagine that the symmetry of these transitions can be broken by introducing a biexciton shift, accounting for any interaction between the excitons in  $|f\rangle$ . However, as we show in App. B, the introduc-

tion of this biexciton shift will be identical for the two transitions  $|i\rangle \rightarrow |f\rangle$  and  $|j\rangle \rightarrow |f\rangle$  which does not actually break the symmetry and the equations remain linearly dependent. The central problem therefore remains: by making the pulses perfectly selective we introduce symmetries into the system which lead to linear dependence which cannot be overcome. In fact, even frequency selective pulses lead to the same issues as outlined above. In order to facilitate the inversion a certain amount of cross-talk between the pulses and states seems to be necessary, in direct contradiction to the requirements of our quantum witness.

Next, we investigated a more realistic system, by considering an ensemble of dimers at random orientations to the light pulses. This leads, within the requirement of near-instantaneous pulses, to excitation of both states with each pulse, i.e., pulse selectivity cannot be perfectly guaranteed generally. This leads to a lifting of the symmetry mentioned above and we have to establish how large the error introduced by the ensuing cross-talk is in our signal expansion and the subsequent inversion.

## 4.2 Isotropic Ensemble Spectroscopy

We have simulated allophycocyanin dimers with varying numbers of phonons according to the protocol set out above, letting the dimer interact with two pulses of light with defined parameters at defined times. The isotropic averaging was done in a 'brute-force' way: by fixing the angle between both site dipole moments ( $40^\circ$ ) the orientation of the dimer was randomised while keeping the polarisation angle between the two pulses (pump and probe) fixed at the magic angle ( $\sim 54.7^\circ$ ). Due to the computational cost involved in these simulations the number of samples varied between the simulations for different number of phonons and qualitative convergence was sought.

Fig. 6 shows the results for the four process matrix elements as a function of delay time,  $\tau$ , and for different numbers of phonons. Also shown is the theoretically predicted result (see Sec. 3.2) and the region of one standard deviation around the curve for 3 phonons (blue shade). We firstly note that the curve for 5 phonons differs numerically from the area containing the cases for 1 - 4 phonons (which is broadly the area of one standard deviation around the 3 phonon case). We attribute this to the fact that the sample size for 5 phonons was significantly smaller than for the other cases due to computational limitations. In fact, the area of one standard deviation around the 5-phonon curve spans an area overlapping with the other curves. We can therefore infer that the calculations are essentially converged with 3 phonons. This is in line with the spectrum shown in Fig. 4, where we can see an overlap of the one-phonon line with the  $|\beta\rangle$  manifold.

While the curves are broadly within the expected regions ( $\chi_{iiii} \simeq 1; \chi_{jjii} \simeq 0$ ) we can see that they do not agree with the theoretically predicted result. In fact, even qualitatively it is hard to justify any agreement. While it is possible that this is due to non-convergence, we are confident that we can rule out this scenario for the reasons discussed above. We have also calculated the NSIT measure for our numerical results and the theoretical prediction (see Fig. 7). Unsurprisingly, we do not find agreement between simulation and theory here either. Studying the form of

the NSIT measure allows us to explain the discrepancy as follows: the NSIT measure provides a witness for the coherence between system states ( $|\alpha\rangle$  and  $|\beta\rangle$ ) which could either be due to dynamics of the system or created by the initial light pulse. In other words, the creation of coherences with the light pulse will lead to a false-positive result in  $W^b$ .

## 4.3 Strong Electronic Coupling

By truncating the vibrational space of each site to one phonon, we limit the sub-space for each 1EM state to eight states, for each excitonic state. In the non-coupled limit ( $\hat{H}_{S-B} = 0$ ) we find the four transitions for  $|\alpha\rangle$  at  $\epsilon_\alpha^{(0)}, \epsilon_\alpha^{(0)} + \omega_a, \epsilon_\alpha^{(0)} + \omega_b, \epsilon_\alpha^{(0)} + \omega_a + \omega_b$  and similarly for the  $|\beta\rangle$  state. Each manifold therefore spans an energy range of  $\omega_a + \omega_b$ , while the energy difference between the vibrational ground states is given by  $2J$ . If we want to minimise the cross-talk between the manifolds then we need to have  $2J \geq \omega_a + \omega_b$  as in this instance the manifolds are well-separated. By defining,

$$r = \frac{2J}{\omega_a + \omega_b}, \quad (37)$$

as the ratio between the electronic and vibrational spacing, we can find that for  $r > 1$  the two spectra are non-overlapping in the uncoupled case. Fig. 8 shows the energy scales involved. For  $\hat{H}_{S-B} \neq 0$  this becomes less-accurate but in the weak-coupling regime is still a useful parameter. We have simulated the hypothetical model for various values of  $r$  and compared to the theoretical prediction of our quantum witness, where we define the deviation parameter,  $\sigma$ , as

$$\sigma = \frac{1}{t_1 - t_0} \frac{\int_{t_0}^{t_1} |\vec{\chi}_{\text{theo}}(t) - \vec{\chi}_{\text{calc}}(t)|^2 dt}{\int_{t_0}^{t_1} |\vec{\chi}_{\text{theo}}(t)|^2 dt}, \quad (38)$$

where  $\vec{\chi}_{\text{theo}}$  and  $\vec{\chi}_{\text{calc}}$  are the theoretical and calculated reduced process tensors, respectively.  $\sigma$  is effectively the average squared deviation over all process tensor elements normalised to the theoretical prediction.

Figure 8 shows the results. As can be seen for  $r > 1$  the results become more accurate, with our signal expansion reproducing the total signal more accurately, as cross-talk is minimised. This underlines our results from Sec. 4.2, i.e., the pulses have to be targeting to a reasonable extent, while not being totally selective. Note also that complete separation of the manifolds leads to trivial excited state dynamics.

## 5 Conclusions

We have presented a quantum witness capable of reporting on the existence of quantum coherences within an electronic system embedded into a vibrational bath, as commonly found in excitonic energy transport in biological systems. The witness relies on partial quantum process tomography of the population-to-population elements at various points during the natural evolution of the excited states and comparing a pure classical path-way of transport to the actual process. It may also be implemented solely with a series of two-pulse pump-probe experiments. Any deviation between these two is then attributed to quantum coherent transport and the witness returns a non-zero value. We then pro-

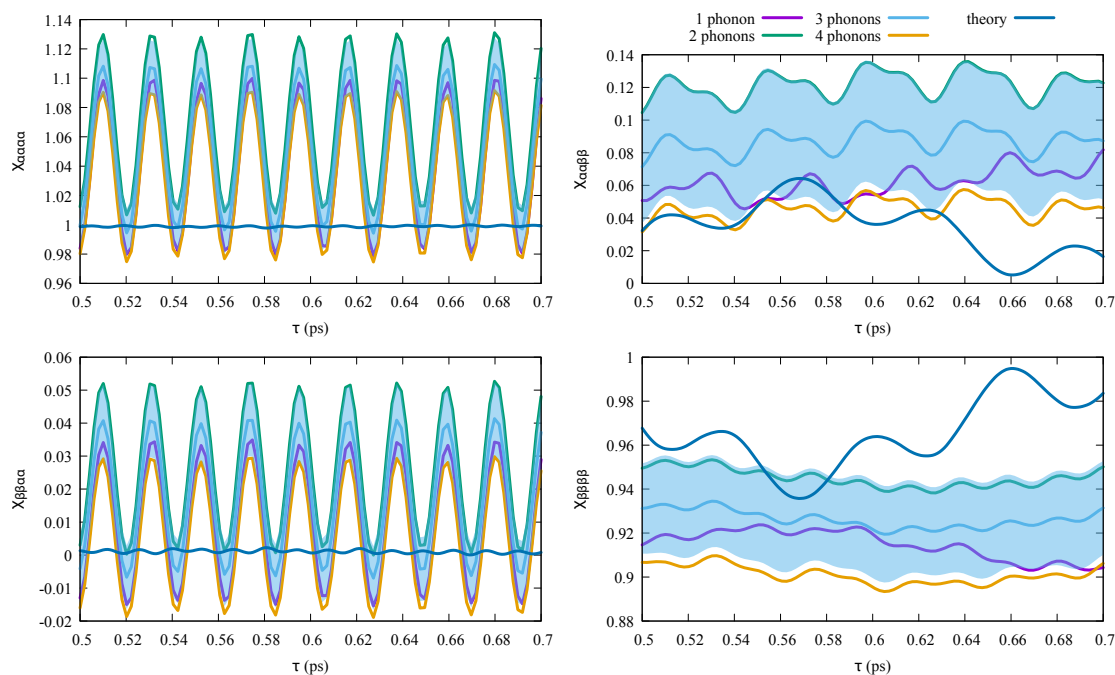


**Fig. 6** Process tensor elements for allophycocyanin dimers as a function of delay time,  $\tau$ , and numbers of phonons. Shown are the results for 1-5 phonons per harmonic oscillator, as well as the theoretically predicted results (dark blue) and the are of one standard deviation around the average for 3 phonons.

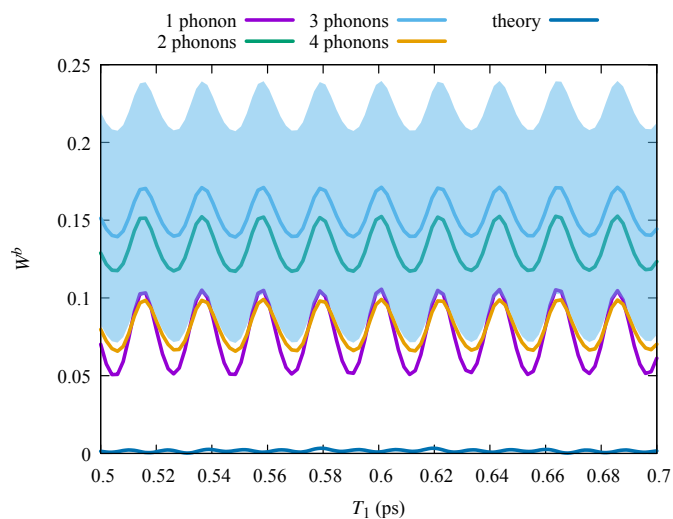


**Fig. 7** NSIT measure for allophycocyanin using the results from Fig. 6 and the theoretical result.

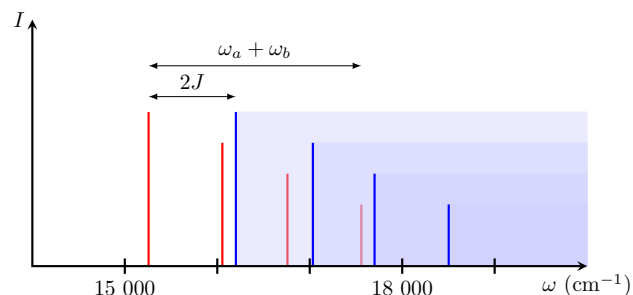


**Fig. 8** Energy scales for allophycocyanin. Changing  $J$  while keeping the vibrational frequencies fixed will shift the two manifold relative to each other, leading to more or less overlap and as a consequence of the targeted pulses to more or less cross-talk between the pulses and manifolds.

ceeded to apply this witness to a coupled dimer system with one vibrational normal mode on each site and simulated the required pump-probe spectra necessary to obtain the required process tensor elements for a single dimer and an isotropic average.

That our quantum coherence witness  $W^b$  is a faithful reflection of  $R(\rho_S)$  rests on certain assumptions. Most significant in the principle of formulating our witness is the Born approximation. We can however still infer the quantum coherence of EET  $R(\rho_S)$  in case of its invalidity using

$$R(\rho_S(t_T)) \geq 2 \left( W^b(t_T; \tau) - \|\gamma_{SB}(t_T)\|_{\text{tr}} - \|\text{tr}_S[\rho_{SB}(t_T)] - \rho_B(t_P)\|_{\text{tr}} \right), \quad (39)$$

if we can lower-bound the violation of the Born approximation and the change in the bath during our spectroscopic protocol. Of course, the system-bath correlations and the bath dynamics

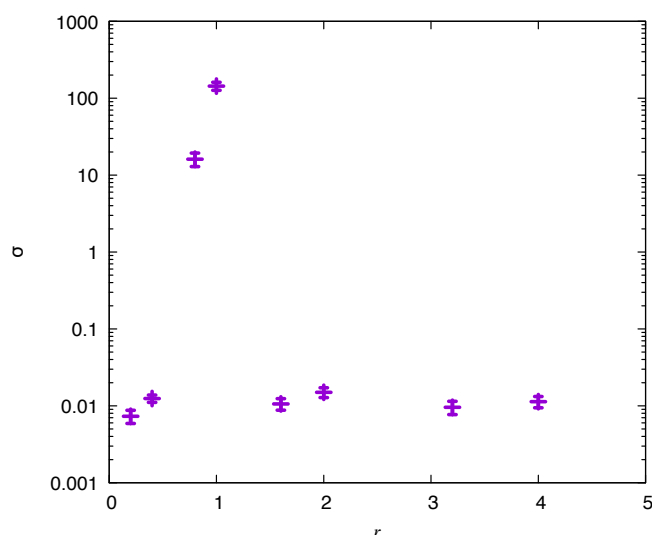


**Fig. 9** Summed squared deviation of the calculated process tensor elements from the theoretical values against the coupling strength parameter,  $r$  (see text). For large  $r$  the deviation shrinks, while for  $r = 1$  the deviation is relatively large. The numerical simulations in this work are performed for  $r = 0.14$ .

have to be small to obtain a non-trivial bound on the excitonic quantum coherence. Recent electronic-vibrational spectroscopic methods<sup>30</sup> may be of use in this regard.

The next significant assumption is the non-invasiveness of the  $\Gamma$  operation. In our spectroscopic protocol, this is implemented using light pulses which are invasive. Not only do they not excise the off-diagonal terms instantaneously but also affect the subsequent dynamics of the systems. This can be addressed experimentally<sup>19,31,32</sup> by designing control experiments that capture the invasiveness of  $\Gamma$  quantitatively.

Another assumption in our derivation of the witness  $W^b$  is that any coherence within the system is generated only by the natural evolution as the witness itself does not discriminate between possible sources of the coherence. This requires temporally narrow pulses to exclude processes induced by the continued interaction with the light field and spectrally narrow pulses to avoid creating coherences between excitonic states with the light itself. Transform limited pulses prohibit this. Time-frequency entangled photon-pairs generated by parametric down-conversion (PDC) may allow simultaneous temporal and spectral resolution that is not possible using any ‘classical’ light source, such as a short laser pulse of broadband thermal-like light<sup>33</sup>. A different strategy of avoiding excitonic coherence creation is to study systems with stronger electronic coupling,  $J$ , that lead to larger separation between the two excitonic states in 1EM. We quantified this in a hypothetical model which showed that stronger electronic coupling leads to a more accurate inversion of the process matrix, while trivialising the excited state dynamics.

All of the above assumptions are violated to varying degrees in our simulations of EET, as they would be in an actual spectroscopic experiment. These will compromise the unambiguity of our quantum coherence witness, if applied blindly. While none of these assumptions are ever likely to be satisfied exactly, we

have discussed how bounding their validity using control and allied characterising experiments can lead towards an unambiguous quantum coherence witness.

## Conflicts of interest

There are no conflicts to declare.

## Acknowledgements

We thank the Engineering and Physical Sciences Research Council, UK (Grant No. EP/K04057X/2) and the Royal Commission for the Exhibition of 1851 for financial support, as well as the CSC, Warwick University, and the Midlands+ HPC for computational support. We also thank Andy Marcus, Jeff Cina, Susana Huelga, Martin Plenio, and Alexandra Olaya-Castro for useful discussions and feedback.

## Notes and references

- 1 G. S. Engel, T. R. Calhoun, E. L. Read, T.-K. Ahn, T. Mančal, Y.-C. Cheng, R. E. Blankenship and G. R. Fleming, *Nature*, 2007, **446**, 782–786.
- 2 M. B. Plenio and S. F. Huelga, *New Journal of Physics*, 2008, **10**, 113019.
- 3 M. Mohseni, P. Rebentrost, S. Lloyd and A. Aspuru-Guzik, *The Journal of Chemical Physics*, 2008, **129**, 174106.
- 4 F. Caruso, A. W. Chin, A. Datta, S. F. Huelga and M. B. Plenio, *The Journal of Chemical Physics*, 2009, **131**, 105106.
- 5 M. M. Wilde, J. M. McCracken and A. Mizel, *Proceedings of the Royal Society A: Mathematical, Physical and Engineering Sciences*, 2010, **466**, 1347–1363.
- 6 E. J. O'Reilly and A. Olaya-Castro, *Nature Communications*, 2014, **5**, 3012 EP.
- 7 J. Yuen-Zhou, J. J. Krich, M. Mohseni and A. Aspuru-Guzik, *Proceedings of the National Academy of Sciences*, 2011, **108**, 17615–17620.
- 8 J. Yuen-Zhou and A. Aspuru-Guzik, *The Journal of Chemical Physics*, 2011, **134**, 134505.
- 9 A. Chenu and G. D. Scholes, *Annual Review of Physical Chemistry*, 2015, **66**, 69–96.
- 10 M. Richter, R. Singh, M. Siemens and S. T. Cundiff, *Science Advances*, 2018, **4**, eaar7697.
- 11 G. D. Scholes, G. R. Fleming, L. X. Chen, A. Aspuru-Guzik, A. Buchleitner, D. F. Coker, G. S. Engel, R. van Grondelle, A. Ishizaki, D. M. Jonas, J. S. Lundeen, J. K. McCusker, S. Mukamel, J. P. Ogilvie, A. Olaya-Castro, M. A. Ratner, F. C. Spano, K. B. Whaley and X. Zhu, *Nature*, 2017, **543**, 647 EP.
- 12 M. Aeschlimann, M. Bauer, D. Bayer, T. Brixner, S. Cunovic, F. Dimler, A. Fischer, W. Pfeiffer, M. Rohmer, C. Schneider, F. Steeb, C. Strüber and D. V. Voronine, *Proceedings of the National Academy of Sciences*, 2010, **107**, 5329–5333.
- 13 M. D. Anderson, S. Tarrago Velez, K. Seibold, H. Flayac, V. Savona, N. Sangouard and C. Galland, *Physical Review Letters*, 2018, **120**, 233601.
- 14 A. J. Leggett and A. Garg, *Physical Review Letters*, 1985, **54**, 857–860.

- 15 C. Emary, N. Lambert and F. Nori, *Reports on Progress in Physics*, 2013, **77**, 016001.
- 16 J. Kofler and Č. Brukner, *Physical Review A*, 2013, **87**, 052115.
- 17 C. Robens, W. Alt, D. Meschede, C. Emary and A. Alberti, *Physical Review X*, 2015, **5**, 011003–.
- 18 L. Clemente and J. Kofler, *Physical Review Letters*, 2016, **116**, 150401–.
- 19 G. C. Knee, K. Kakuyanagi, M.-C. Yeh, Y. Matsuzaki, H. Toida, H. Yamaguchi, S. Saito, A. J. Leggett and W. J. Munro, *Nature Communications*, 2016, **7**, 13253 EP.
- 20 T. Baumgratz, M. Cramer and M. B. Plenio, *Physical Review Letters*, 2014, **113**, 140401.
- 21 I. Marvian and R. W. Spekkens, *Physical Review A*, 2016, **94**, 052324.
- 22 L. Valkunas, D. Abramavicius and T. Mančal, *Molecular Exciton Dynamics and Relaxation*, Wiley-VCH, Berlin, 1st edn, 2013.
- 23 G. C. Knee, M. Marcus, L. D. Smith and A. Datta, *Phys. Rev. A*, 2018, **98**, 052328.
- 24 C.-M. Li, N. Lambert, Y.-N. Chen, G.-Y. Chen and F. Nori, *Scientific reports*, 2012, **2**, 885; 885–885.
- 25 W. Barford and O. R. Tozer, *The Journal of Chemical Physics*, 2014, **141**, 164103.
- 26 M. Marcus, O. R. Tozer and W. Barford, *J. Chem. Phys.*, 2014, **141**, 164102.
- 27 W. Barford and M. Marcus, *J. Chem. Phys.*, 2017, **146**, 130902.
- 28 J. Yuen-Zhou, J. J. Krich, I. Kassal, A. S. Johnson and A. Aspuru-Guzik, *Ultrafast Spectroscopy*, IOP Publishing, 2014.
- 29 S. V. Moreira and F. L. Semião, *Quantum Science and Technology*, 2019, **4**, 03LT01.
- 30 T. A. A. Oliver, N. H. C. Lewis and G. R. Fleming, *Proceedings of the National Academy of Sciences*, 2014, **111**, 10061–10066.
- 31 A. J. Leggett, *Foundations of Physics*, 1988, **18**, year.
- 32 M. M. Wilde and A. Mizel, *Foundations of Physics*, 2012, **42**, 256–265.
- 33 M. G. Raymer, A. H. Marcus, J. R. Widom and D. L. P. Vitullo, *The Journal of Physical Chemistry B*, 2013, **117**, 15559–15575.

## A Computational Details

In order to simulate the spectroscopic experiments we directly integrated the time-dependent Schrödinger equation by adding the time-dependent light field described by Eq (23) originating from the two pulses in a two-pulse pump-probe experiment and using the resulting Hamiltonian to evolve a state initialised in the true (i.e. electronic and vibrational) groundstate. The observable we are interested in is the change of intensity of this light field as it interacts with the sample. As we use a classical light field we have to track these changes indirectly by monitoring the changes in populations of the different states of the electronic system. For instance, a net loss of population in the ground state during one

integration time-step corresponds to a loss in intensity of the light pulse due to absorption, while a net-loss in the 2EM shows emission (as we do not consider any electronic states above 2EM). By keeping track of these changes it is possible to simulate a time-resolved signal as is would be recorded in a single-molecule experiments under the simulated conditions.

The direct simulation of the two-pulse experiment acting on one molecule requires a careful consideration of the relative phase of the two fields experienced by the molecule. Depending on the spatial positioning the molecule will experience slightly different phase-shifts. While automatically taken care off in real-space simulations, we do not consider the position of the molecule explicitly so the differences in the phase has to be incorporated directly into the simulation. One way would be to introduce a random phase-shift in each simulation and averaging out the relative phase differences in this way. However, computational cost can be reduced by considering the same molecule with two different phase shifts: 0 and  $\pi$ . In this way we simulate each molecule experiencing an average field instead of averaging over molecules experiencing slightly different phase shifts.

The observable studied in two-photon pump-probe spectroscopy is the signal due to the excited state. As such the contribution to the signal from the ground state has to be subtracted. To this purpose we simulate the response of the molecule to the probe pulse only. The difference between the phase-averaged signal from the full pump-probe simulation and the probe-only will then give the required time-resolved signal due to the excited state transitions. Integrating these signals lastly gives rise to the integrated signal required for the inversion in Eq. (32).

Lastly, to average over the relative orientation of the sample dipole to the light polarisation the latter is kept fixed while the sample is oriented randomly with a fixed angle between the site dipoles in order to simulate a bound dimer system.

## B Polarisation-Selective Pulses

In the case of single molecule/dimer spectroscopy the pulses can be chose such that one transition is dark by ensuring the polarisation is aligned with one and perpendicular to the other transition dipole moment, i.e. we need to ensure that the system under investigation has orthogonal dipole moments for the two states of the 1EM. We can write,

$$\mu_{\chi} = \sum_i \chi_i \mu_i, \quad (40)$$

where  $\chi$  is the energetic eigenstate and  $\chi_i$  is the associated wave-function in the site-basis.  $i$  runs over the sites. Then,

$$\mu_{\chi} \cdot \mu_{\chi'} = \sum_{ij} \chi_i \chi'_j \mu_i \cdot \mu_j. \quad (41)$$

For a dimer this can be re-written as,

$$\mu_{\alpha} \cdot \mu_{\beta} = [\alpha_a \beta_b + \alpha_b \beta_a + \alpha_a \beta_a + \alpha_b \beta_b] \mu_a \cdot \mu_b. \quad (42)$$

For any dimer we find that  $\alpha_a = \beta_b$  and  $\alpha_b = -\beta_a$  and hence,

$$\mu_{\alpha} \cdot \mu_{\beta} = [|\alpha_a|^2 - |\alpha_b|^2] \mu_a \cdot \mu_b. \quad (43)$$

In order for the two transition dipole moments to vanish we therefore either need a homodimer ( $\alpha_a = \alpha_b \Rightarrow \epsilon_a = \epsilon_b$ ) or we need the two sites constituting the dimer to have orthogonal dipole moments.

This has direct consequences for the calculation of the transition probabilities. We can write,

$$\Pi_{ij}^p = \left\{ \frac{\mu_{ij} \cdot \mathbf{e}_p}{\hbar} \exp \left[ -\frac{(\Delta E_{ij} - E_p)^2}{2\sigma_p^2} \right] \right\}^2. \quad (44)$$

However, if the pulses are in resonance with the transition and the pulses are perfectly selective by polarization then  $\Delta E_{ij} - E_p = 0$  and  $\mu_{ij} \cdot \mathbf{e}_p = \mu_{ij} \eta_p$ , where  $\eta_p$  is the intensity of the pulse  $p$ . Consequently,

$$\Pi_{ij}^p = \left( \frac{\mu_{ij} \eta_p}{\hbar} \right)^2. \quad (45)$$

It then follows, for two perfectly polarization selective pulses that, in order for Eqs. (34) and (35) to be linearly independent we require,

$$\mu_{fi}^2 \mu_{fj}^2 \neq \mu_{gi}^2 \mu_{gj}^2, \quad (46)$$

but  $\mu_{gi} = \mu_i = \mu_{fj}$  and  $\mu_{gj} = \mu_j = \mu_{fi}$  and hence,

$$\mu_i^2 \mu_j^2 \neq \mu_i^2 \mu_j^2, \quad (47)$$

which cannot be true and therefore the inversion fails.

## C Biexciton Shift

The introduction of a biexciton shift will lift the degeneracy of the transitions from the ground state to the 1EM and from the 1EM to the 2EM. for instance, if  $E_g = 0$  then  $\Delta E_{ig} = E_i$  but  $\Delta E_{fj} = E_i + \delta E$ , where  $\delta E$  quantifies the interaction between two excitations on the dimer. As a direct consequence, the probe pulse won't be resonant with the transition to the 2EM if it is resonant with the transitions to the 1EM and will therefore change the transition probability amplitudes. In order for Eqs. (34) and (35) to be linearly independent we require,

$$\Pi_{fi}^{-P} \Pi_{fj}^P \neq \Pi_{gi}^{-P} \Pi_{gj}^P. \quad (48)$$

Assuming equivalence between transition dipole moments as above and that  $\eta_p = \eta_{-p}$  as well as  $\sigma_p = \sigma_{-p}$  (i.e. the only adjustable parameters of the pulses are polarization and central frequency) then this reduces to,

$$(\Delta E_{fi} - E_{-P})^2 - (\Delta E_{gj} - E_{-P})^2 \neq (\Delta E_{fj} - E_P)^2 - (\Delta E_{gi} - E_P)^2. \quad (49)$$

While  $E_{gi} = E_P$  and  $E_{gj} = E_{-P}$ , the biexciton shift will introduce an offset, i.e.,  $\Delta E_{fj} - E_P = \delta E$  and  $\Delta E_{fi} - E_{-P} = \delta E$ . However, this does not fulfil Eq. (48) as it leads to  $\delta E \neq \delta E$  and as such the biexciton shift does not lead to linearly dependent equations, causing the inversion to fail, as well.